Biophysical Journal, Volume 96

Supporting Material

A kinetic model of the inositol trisphosphate receptor based on single-channel data

Elan Gin, Martin Falcke, Larry E. Wagner II, David I. Yule, and James Sneyd

A kinetic model of the inositol trisphosphate receptor based on single-channel data. Supplementary material.

Elan Gin
Department of Mathematics,
The University of Auckland, Auckland, New Zealand

Martin Falcke
Max Delbrück Centre for Molecular Medicine,
Robert Rössle Str. 10, 13902 Berlin, Germany

Larry E. Wagner II
Department of Pharmacology and Physiology,
University of Rochester Medical Center, Rochester, NY 14642

David I. Yule
Department of Pharmacology and Physiology,
University of Rochester Medical Center, Rochester, NY 14642

James Sneyd [1]
Department of Mathematics,
The University of Auckland, Auckland, New Zealand

[1]Corresponding author. Address: Department of Mathematics, The University of Auckland, Private Bag 92019 Auckland, New Zealand Tel.: (649)373-7599, Fax: (649)373-7457

1 Distinguishing between equivalent steady-state models

We simulated activation latency data from our two models using the mean fitted rate constants. We first started with the [Ca^{2+}] at 50 nM, and then "stepped" up the concentration to 200 nM. We assumed the receptor was at steady-state at 50 nM, and therefore calculated the steady-state occupancies for each of the four states at this concentration. For Model 1, the steady-state occupancy is approximately [$C_{1_{SS}}$, $C_{2_{SS}}$, $C_{3_{SS}}$, $O_{4_{SS}}$] = [0.0005 0.003 0.991 0.0055] and for Model 2, [$C_{1_{SS}}$, $C_{2_{SS}}$, $C_{3_{SS}}$, $O_{4_{SS}}$] = [0.942 0.041 0.005 0.012]. We then used the Gillespie algorithm to simulate approximately 1000 times to first opening after an increase to 200 nM [Ca^{2+}]. The distribution of the times to first opening is plotted in Fig. S1, with the theoretical pdfs, calculated from the fitted rate constants, superimposed. For Model 1, the time to first opening is much shorter than for the Model 2, with the mean time approximately 12 ms whereas for the second model, the mean time is approximately 55 ms. This is due to the different "route" to the open state. At steady-state, for both models, the receptor is mainly in the long closed state (C_3 for Model 1 and C_1 for Model 2). Once the [Ca^{2+}] is stepped up to 200 nM, the receptor opens. For Model 1, the time to first opening is via the route $C_3 \rightarrow C_2 \rightarrow O_4$, corresponding to long closed time → short closed time. For Model 2, the time to first opening is the route $C_1 \rightarrow C_2 \rightarrow O_4$, corresponding to long closed time → medium closed time. Therefore, this type of non-steady-state data could be used in addition to steady-state data, to determine a more precise model of the IPR.

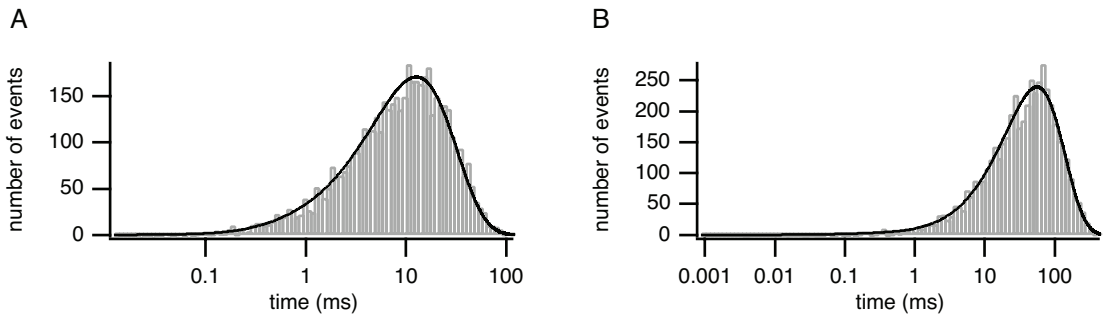

Figure 1: Distributions of times to first opening after a step up from 50 nM [Ca^{2+}] to 200 nM [Ca^{2+}]. A: Model 1. B: Model 2.

2 Effects of phosphorylation and dependence on agonist

We use data from two IPR mutants to investigate the effects on IPR activity by phosphorylation and adenophostin concentration. The experimental data used to illustrate the fitting methods are steady-state single-channel data obtained from the type-1 IPR. Two mutants were constructed by Wagner et al. (1, 2) to study phosphorylation of the receptor by cAMP (PKA) and cGMP (PKG). A non-phosphorylatable mutant, called the AA mutant, was constructed by mutating two serine residues to alanine residues. Substituting two glutamate residues for serine residues in phosphorylation sites of the IPR gave the EE mutant, which mimics an IPR that is permanently phosphorylated. Studies by Wagner et al. (1, 2) of measurements of $[Ca^{2+}]$ using fluorescent indicators showed that the EE mutant has markedly enhanced IP_3-induced Ca^{2+}. However, the $[Ca^{2+}]$ measurements using fluorescent dyes provide limited mechanistic information on the effects of phosphorylation on channel gating at a single-channel level. Thus the whole-cell mode of the patch-clamp technique (3) was utilised. The mutants were expressed in DT40 cells lacking expression of all IPR types. The ability to express the mutant constructs on a null background and study their single channel behaviour is a powerful tool, able to give insight into the regulation of the IPR in a native environment. By comparing the gating characteristics of the two mutants, Wagner et al. (4) showed that PKA phosphorylation results in an increase in the open probability of the IPR. The experimental protocol and further results can be found in Wagner et al. (4).

The experiments were done using adenophostin A as the agonist. Adenophostin A is a high affinity IPR agonist and activates the channel by binding to the IP_3-binding site. The agonist dependency for the EE and AA mutants was investigated at 200 nM $[Ca^{2+}]$ and 5 mM [ATP] with the agonist concentration between 20 and 10000 nM. By using data obtained at various agonist concentrations, we are able to characterise each of the rate constants as a function of agonist concentration and in doing so, identify which transitions are most affected by agonist. In addition, by comparing the results of the AA and EE mutants, we can also determine which transitions are most affected by phosphorylation, and how.

We will fit the Markov model shown in Fig. S2.

The fitted steady-state open probabilities for the AA and EE mutants, as functions of agonist concentration, are shown in Fig. S3. The AA open probability is given by the solid curve with square symbols, the EE open probability is the dashed curve with circle symbols. The experimental open probabilities have a similar maximum value for both mutants, with the effect of phosphorylation shifting the agonist dependency to a lower concentration range.

To find the model steady-state open probability, we use mass action kinetics to write

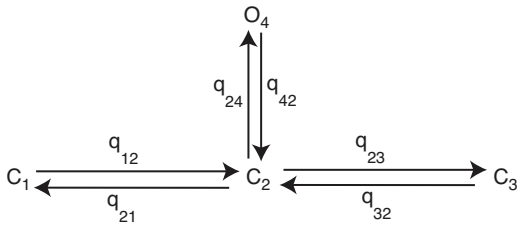

Figure 2: Four-state Markov model. Closed states are C_1, C_2 and C_3, open state is O_4. Rate constants are q_{ij}, giving the transition rate from state i to state j. The units are ms^{-1}.

down the system of differential equations governing the state dynamics:

$$\frac{dC_1}{dt} = -q_{12}C_1 + q_{21}C_2, \quad (1)$$

$$\frac{dC_2}{dt} = q_{12}C_1 - (q_{21} + q_{23} + q_{24})C_2 + q_{32}C_3 + q_{42}O_4, \quad (2)$$

$$\frac{dC_3}{dt} = q_{23}C_2 - q_{32}C_3, \quad (3)$$

with

$$O_4 = 1 - (C_1 + C_2 + C_3). \quad (4)$$

The steady-state solution is found by setting the system of differential equations equal to zero. The analytic expression for the steady-state open probability is

$$O_4 = \frac{q_{12}q_{32}q_{24}}{q_{12}q_{32}q_{24} + q_{42}q_{23}q_{12} + q_{42}q_{32}q_{12} + q_{42}q_{32}q_{21}}. \quad (5)$$

In order to calculate the model steady-state open probability as a function of agonist concentration, it is necessary first to calculate how each of the rate constants depends on the adenophostin concentration. Results from the fit are shown in Fig. S4. Although there is considerable variability, some patterns are apparent. Three of the rates, q_{12}, q_{24}, and q_{42} appear not to depend on agonist concentration, and we model these as constants by setting them at their mean values. Although the other three rates are clearly functions of agonist concentration, we have data at only a relatively small number of concentrations, and thus it is impossible to determine the exact functional dependence.

However, if we assume that the agonist-dependency of the EE rate constants can be fitted by a shift in agonist-sensitivity of the AA agonist-dependency curves we obtain reasonable continuous models for both sets of rate constants (Fig. S4, solid curves). We chose to fit Hill functions to q_{21}, q_{23} and q_{32} for the AA mutant, with Hill coefficients of three. The functions for the EE mutant are the same as for the AA mutant, with a shift in the agonist dependency. From Fig. 4 we see that our hypothesis is consistent with

the rate constant estimates. The other rate constants are assumed to be independent of agonist concentration, and have the same value for both mutants.

Standard deviations are plotted, and in some cases, the bars are narrower than the plotting symbols used. A pooled standard deviation formula is used, which assumes that though the means can be different, the standard deviations of the individual cells are similar. It is given by

$$s_p = \sqrt{\frac{\Sigma_{i=1}^{k}((n_i-1)s_i^2)}{\Sigma_{i=1}^{k}(n_i-1)}},$$

where there are k cells and there are n iterations for each cell. The s_i are the individual standard deviations for each cell. Therefore, the narrow standard deviations shown are a result of small standard deviations in the individual fits. The number of experiments fitted at each concentration for the AA data are $N = 5, 3$ and 4, respectively. For the EE data, we only have one set of fitted values at 100 nM as other experiments contained either no activity or the fits were poor. However, we assume that phosphorylation simply shifts the agonist sensitivity, and thus, we can shift the AA fits to obtain EE fits.

Letting $a =$ [agonist], the rate constants for both mutants are:

$$\begin{aligned} q_{21}(a) &= \frac{V_{21}}{1+\alpha_{21}k_{21}a^3} + b_{21}, \\ q_{23}(a) &= \frac{V_{23}}{1+\alpha_{21}k_{23}a^3} + b_{23}, \\ q_{32}(a) &= \frac{\alpha_{32}V_{32}a^3}{1+\alpha_{32}k_{32}a^3} + b_{32}. \end{aligned}$$

where the values α_{21}, α_{23} and α_{32} give a shift in the agonist dependency and are different for the two mutants. Parameter values are given in Table 1. Agonist-independent rate constants are $q_{12} = 0.7$ ms^{-1}, $q_{24} = 7$ ms^{-1}, $q_{42} = 2.7$ ms^{-1}.

	V_{21}	0.0949 nM^{3}ms^{-1}	k_{21}	5×10^{-10} nM^{-3}	b_{21}	0.085 ms^{-1}
	V_{23}	0.162 nM^{3}ms^{-1}	k_{23}	5×10^{-9} nM^{-3}	b_{23}	0.001 ms^{-1}
	V_{32}	3×10^{-12} nM^{-3}ms^{-1}	k_{32}	1.5×10^{-10} nM^{-3}	b_{32}	0.0007 ms^{-1}
AA	α_{21}	1	α_{23}	1	α_{32}	1
EE	α_{21}	6000	α_{23}	2000	α_{32}	1500

Table 1: Agonist-dependent rate constant parameter values. Parameter values are identical for the AA and EE mutants except for the α_{ij}.

Once we have the rate constants expressed as continuous functions of a, we can then plot the theoretical open probability of the IPR, as a function of a. These curves are shown in Fig. S4 as solid lines, and agree well with the experimental data, as expected.

From the fitted continuous function, we can see that the increased open probability at higher agonist concentrations is a result of the decreased number of longer closed times,

C_3, and an increase in the transition rate to the short closed state C_2, the only state from which the open state can be reached. The rate constant q_{24} remains constant over the adenophostin concentration range, and therefore does not affect the open probability of the IPR. Similarly, there is no change in the mean open time, $1/q_{42}$, and therefore the open probability is not increased by longer excursions in the open state.

This implies that the processes that open the IPR are independent of adenophostin and thus, presumably, of IP_3. The effect of adenophostin is to increase the probability that the IPR is in a state that is capable of opening. In other words, adenophostin "primes" the IPR. This is accomplished in two ways; as the adenophostin concentration increases, the transition rates from C_2 to C_1 and C_2 to C_3 decrease, and the transition rate from C_3 to C_2 increases. Both these effects increase the probability the IPR is in state C_2, thus increasing the open probability.

Here, we construct a Markov model where the rates are merely given by heuristic increasing or decreasing functions; clearly values at more agonist concentrations are required to fully characterise the dependencies. No biophysical derivation of these rates is given, and we cannot, as mentioned above, propose any more complex model from which the current simple model can be derived. The heuristic rate functions used are all rational functions of the agonist concentrations, which are consistent with either a pseudo-steady-state derivation, or an equilibrium approximation, but more than that is impossible to claim without constructing a more detailed model. Since the choice of polynomial function used has no effect on the data, using different functions will have no effect on our conclusions about the effects of phosphorylation and also concentration changes. By using Hill functions, we can also model the effects of phosphorylation by a shift in the agonist sensitivity (given by the α_{ij}) while ensuring the rate constants remain positive.

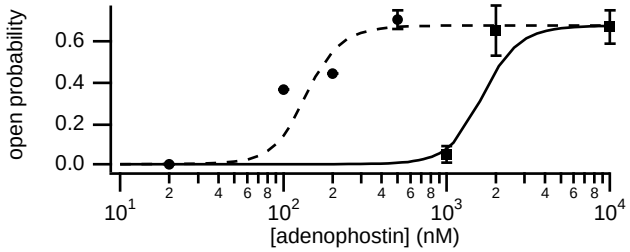

Figure 3: Fitted steady-state open probability as a function of agonist for the AA and EE mutants. Standard deviations are shown. EE: dashed curve with circle symbols; AA: solid curve with square symbols.

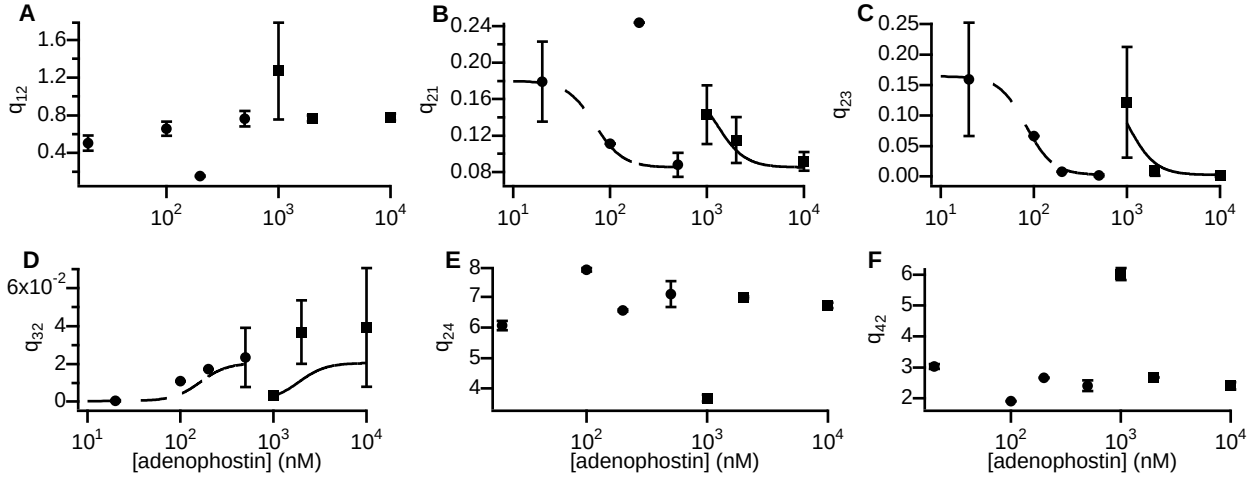

Figure 4: Fitted AA and EE rate constants as functions of agonist concentration. EE: dashed curve with circles; AA: solid curve with square symbols. The smooth lines are obtained by fitting Hill functions to the fitted rate constants, and assuming that the fit to the EE data is merely a shifted version of the fit to the AA data.

3 Response to step increases in $[Ca^{2+}]$

Model 1 was used to predict the response to step increases in $[Ca^{2+}]$ (Fig. S5). When $[Ca^{2+}]$ is held fixed at a low steady-state concentration ($[Ca^{2+}]$ = 10 nM) the IPR is mostly in state C_3. When $[Ca^{2+}]$ is increased and held fixed at a new value, the open probability of the IPR increases monotonically to its new value.

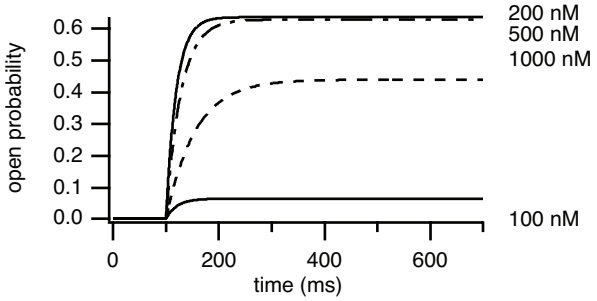

Figure 5: Model open probability response to step increases in $[Ca^{2+}]$ from a low steady-state of 10 nM. Step increases to: 100 nM (bottom, solid curve), 200 nM (top, solid curve), 500 nM (dashed-dotted curve), 1000 nM (dashed curve).

References

1. Wagner, L. E., II, W.-H. Li, and D. I. Yule, 2003. Phosphorylation of type-1 inositol 1,4,5-trisphosphate receptors by cyclic nucleotide-dependent protein kinases. *J. Biol. Chem.* 278:45811–45817.

2. Wagner, L. E., II, W.-H. Li, S. K. Joseph, and D. I. Yule, 2004. Functional consequences of phosphomimetic mutations at key cAMP-dependent protein kinase phosphorylation sites in the type 1 inositol 1,4,5-trisphosphate receptor. *J. Biol. Chem* 279:46242–46252.

3. Dellis, O., S. G. Dedos, S. C. Tovey, Taufiq-Ur-Rahman, S. J. Dubel, and C. W. Taylor, 2006. Ca^{2+} entry through plasma membrane IP_3 receptors. *Science* 313:229–233.

4. Wagner, L., II, S. Joseph, and D. Yule, 2008. Regulation of single inositol 1,4,5-trisphosphate receptor channel activity by protein kinase A phosphorylation. *J. Physiol.* 586:3577–3596.